



**INTEGRATED OPTICAL MACH-ZEHNDER
INTERFEROMETER FOR BIOSENSOR
APPLICATION**

by

KHOR KANG NAN

(1130110614)

A thesis submitted in fulfillment of the requirements for the degree of
Master of Science (Microelectronic Engineering)

**School of Microelectronic Engineering
UNIVERSITI MALAYSIA PERLIS**

2015

**GRADUATE SCHOOL
UNIVERSITI MALAYSIA PERLIS**

PERMISSION TO USE

In presenting this thesis in fulfillment of a post graduate degree from Universiti Malaysia Perlis, I agree that permission for copying of this thesis in any manner, in whole or in part, for scholarly purposes may be granted by my supervisor or, in their absence, by Dean of the Graduate School. It is understood that any copying or publication or use of this thesis or parts thereof for financial gain shall not be allowed without my supervisor's written permission. It is also understood that due recognition shall be given to me and to Universiti Malaysia Perlis for any scholarly use which may be made of any material from my thesis.

Requests for permission to copy or make other use of material in whole or in part of this thesis are to be addressed to:

**Dean of Centre for Graduate Studies
Universiti Malaysia Perlis
No. 112 & 114, Tingkat 1, Blok A, Taman Pertiwi Indah
Jalan Kangar-Alor Setar, Seriab
01000 Kangar
Perlis Indera Kayangan
Malaysia**

ACKNOWLEDGEMENTS

I would like to express my deepest gratitude to my supervisor, Dr Mukhzeer Mohamad Shahimin for his assistance, patience and continued support throughout my project. His guidance has been essential to the progress of this project.

I would like to thank the staff of University of Malaysia Perlis, School of Microelectronic Engineering, Institute Nanoelectronic Engineering (INEE), School of Material Engineering for their endless help in my project.

I also extend my special thanks to my family; my parents; Khor Hee Chuan and Heng Lang Hwang who have been tireless in giving me moral support and whom always pray for my success. I would like to thank my friend who have accompanied and supported me which had made my life bearable. Special thank to my girlfriend, Chong Pei Tee who has been supportive and patience throughout my project.

TABLE OF CONTENTS

	PAGES
DECLARATION OF THESIS	ii
COPYRIGHT	iii
ACKNOWLEDGEMENTS	iv
TABLE OF CONTENTS	v
LIST OF TABLES	viii
LIST OF FIGURES	ix
LIST OF NOMENCLATURE	xiv
LIST OF SYMBOLS	xvii
ABSTRAK	xxi
ABSTRACT	xxii
CHAPTER 1: INTRODUCTION	
1.1 Background	1
1.2 Problem Statement	11
1.3 Research Aim and Objectives	14
1.4 Research Approach, Scope and Limitation	15
1.5 Thesis Organization	16
CHAPTER 2: LABEL-FREE OPTICAL BIOSENSOR FOR IDEAL SURVEILLANCE RDT	
2.1 Introduction	18
2.2 Overview of Biosensor	19
2.3 Biomarkers of Dengue Diagnosis	22
2.4 Ideal Surveillance Rapid Diagnostic Test	27
2.5 Review on Dengue Biosensor	30
2.5.1 Piezoelectric Transducer	30
2.5.2 Fluorescent Spectroscopy	32

2.5.3	Fiber Optic	33
2.5.4	Surface Plasmon Resonance	35
2.5.5	Surface Photonic Crystal	37
2.5.6	Magnetic Bead Counter	37
2.5.7	Raman Spectroscopy	39
2.5.8	Comparison of Existing Dengue Biosensor	40
2.6	Fundamental of Integrated Optic for Evanescent Field Sensing	42
2.6.1	Optical Waveguide Theory	44
2.6.1.1	Total Internal Reflection	45
2.6.1.2	Transverse Resonance Condition	46
2.6.2	2D Mode Solver	48
2.6.3	Evanescent Field Sensing	52
2.7	Advantages of Integrated Optical Mach-Zehnder Interferometer (IO-MZI) Biosensor	55
2.8	Principal of IO-MZI Biosensor	59
2.9	Detection Limit of IO-MZI Biosensor	63
2.9.1	Sensitivity of IO-MZI Biosensor	64
2.9.2	Minimum Detectable Phase Change of IO-MZI Biosensor	66
2.10	Optimization of IO-MZI Biosensor	68
2.11	Discussion	75

CHAPTER 3: METHODOLOGY

3.1	Introduction	78
3.2	Introduction to OptiBPM	78
3.3	Simulation Configuration	83
3.4	Simulation Process Flow	84
3.5	Design of Rib Waveguide	85
3.5.1	Modal Behaviour	85
3.5.2	Evanescent Field Penetration Depth	86
3.5.3	Bulk Sensitivity	87
3.5.4	Leakage Loss	88
3.5.5	Selection of Rib Waveguide Configuration	88
3.6	Design of Y-branch Splitter	89

3.7	Design of Mode Size Converter	89
3.8	Design of IO-MZI	90

CHAPTER 4: RESULT AND DISCUSSION

4.1	Rib Waveguide	93
4.1.1	Modal Behaviour	93
4.1.2	Evanescence Field Penetration Depth	94
4.1.3	Bulk Sensitivity	95
4.2	Y-Branch Splitter	100
4.3	Mode-Size Converter	101
4.4	Optimized IO-MZI Biosensor	103
4.5	Discussion	104

CHAPTER 5: CONCLUSION AND FUTURE WORKS

5.2	Conclusion	106
5.3	Future works	108

REFERENCES	109
-------------------	-----

APPENDIX	118
-----------------	-----

LIST OF TABLES

TABLE		PAGE
2.1	Type of Transduction mechanism and the corresponding Label-free detection method	25
2.2	WHO – Ideal characteristics of surveillance RDT (Mabey et al., 2004)	15
2.3	Summary of dengue biosensor in term of detection limit, biomarkers, time and equipment	41
2.4	Comparison of effective index obtained by using the in-house 2D mode solver and the commercial OptiWave 2D mode solver	57
2.5	Advantages of integrated optical Mach-Zehnder Interferometer biosensor compared to other biosensors	45
2.6	Methods to increase sensitivity of IO-MZI biosensor	71
2.7	Comparative study of IO-MZI biosensor of different interaction length, waveguide material, thickness, wavelength and polarization in term of detection limit, sensitivity and minimum detectable phase change	72
3.1	The component of IO-MZI included in the simulation with the aim and the related design parameters	83
4.1	Optimized design parameters and the corresponding loss for rib waveguide, Y-branch splitter, mode-size converter and IO-MZI for WG_75 and WG_250 respectively	102
5.1	Comparison of performance of various IO-MZI biosensor configurations with current work	108

LIST OF FIGURES

FIGURE		PAGE
1.1	Urban cycle (b) of dengue virus (DENV) (a) transmission between <i>Aedes aegyti</i> (c) and humans (Whitehead et al., 2007).	2
1.2	Distribution of countries or areas at risk of dengue transmission, worldwide, 2008 with the corresponding co-circulating serotypes. (Maria G. Guzman et al., 2010; WHO, 2008)	3
1.3	Number of dengue cases reported to World Health Organization from 1955 – 2007. (WHO, 2009)	4
1.4	Incidence rate of dengue in Malaysia. Estimated case is referred the estimated actual case with the expansion factor of 3.42 (Shepard et al., 2013)	5
1.5	Ideal surveillance model based on survey and recommendation carried out by Gubler et al, Runge-Ranzinger et al. and PDVI. Size of circle indicate the importance of the surveillance elements	9
1.6	Example of commercial (a) ELISA kit and (b) immunochromatography rapid diagnostic test (ICT-RDT)	13
1.7	Sensitivity and specificity of commercial immunochromatographic rapid diagnostic tests (RDT) for rapid dengue diagnosis.	14
2.1	Elements of biosensor for Point of Care (POC) diagnostic. (Vasan et al.)	19
2.2	Primary biomarkers for dengue diagnosis and the corresponding period for sensitive detection. (Rosanna W. Peeling et al., 2010)	23
2.3	Immunoassay to detect IgG (a), IgM (b) and NS1 (c)	27
2.4	Ideal surveillance rapid diagnostic test for dengue surveillance	28
2.5	Ultimate lab-on-a-chip for point-of-care diagnostic (Tudos et al., 2001)	30

2.6	Schematic of flow injection system for immunology characterization. Inset shows the structure of 10MHz QCM formed by 8mm AT quartz wafer sandwiched by 4mm gold electrode (T. Z. Wu et al., 2005)	31
2.7	(a) Magnetic particle based immunoassay for dengue biomarker detection. (b) Schematic of PDMS based microfluidic system (Y. F. Lee et al., 2009).	33
2.8	Chemiluminescent optical fiber immunosensor (OFIS) for dengue diagnostic. Chemiluminescent signal produced from reduction of HRP is reflected into optical fiber tip and detected by a photomultiplier tube (PMT) (Atias et al., 2009)	34
2.9	Dengue specified IgM antibody detection based on surface Plasmon resonance technique provided by Biacore (Jahanshahi et al., 2014). The inset shows the immuno chip that contains slab SPR waveguide (gold layer) for SPR sensing.	35
2.10	Integrated optical biosensor with LSPR channel waveguide: (a) top view of the biosensor and (b) cross section of the LSPR channel waveguide (Wong et al., 2014)	36
2.11	Magnetic bead bioassay platform for dengue detection: (a) CMOS manufactured hall sensor to detect the quantity of magnetic bead with integrated amplifier and signal processing circuit and (b) reader system consist of custom electromagnet triggered by computer. AC signal is generated to trap the magnetic bead while DC signal is generated for magnetic washing. (Aytur et al., 2006)	38
2.12	Total internal reflection of electromagnetic wave within waveguide: (a) planar waveguide and (b) channel waveguide	43
2.13	a) Asymmetric planar waveguide with the total internally reflected optical ray zigzagging along waveguide. (b) Two orthogonal component of propagating optical ray namely transverse wavevector, k_x and longitudinal wavevector, β . Optical rays must fulfill Two conditions for mode formation: 1) total internal reflection and 2) transverse resonance condition	45
2.14	Effective index as function of thickness for the 6 lowest waveguide mode of silicon nitride planar waveguide ($n_c = 1.33$, $n_g = 2.0$, and $n_s = 1.46$) with wavelength of 633nm for TE and TM polarization. Mono-mode region and multi-mode region is defined by the cut-off thickness of first-	49

	order mode	
2.15	MATLAB numerical solution of the waveguide mode effective index for silicon nitride waveguide ($N_c = 1.33$, $N_g = 2.0$, and $N_s = 1.46$) with a thickness of 1000nm and TE-polarized light with a wavelength of 633nm. (a) Graphical solution of transverse resonance condition of waveguide for TE and TM-polarization light. (b) Number of mode and the regarding effective index.	50
2.16	Modal distribution of fundamental mode for silicon nitride planar waveguide ($N_c = 1.33$, $N_g = 2.0$, and $N_s = 1.46$) with thickness of 1000nm and wavelength of 633nm	51
2.17	Evanescent field sensor for the application of bio-molecules detection.	52
2.18	Calculated Bulk sensitivity and Surface sensitivity for silicon nitride planar waveguide ($N_c = 1.33$, $N_g = 2.0$, and $N_s = 1.46$) as function of thickness with wavelength of 633nm.	54
2.19	Schematic of integrated optical Mach-Zehnder Interferometer (Prieto et al., 2003).	55
2.20	Integration of LED (excitation element) and photodetector (readout element) with IO-MZI biosensor (sensing chip). (Misiakos et al., 2013)	57
2.21	Basic structure of integrated optical Mach-Zehnder interferometer (IO-MZI) biosensor. Left inset shows the rib waveguide structure and corresponding modal distribution. Right inset shows the typical output response of IO-MZI biosensor	59
2.22	Output response of IO-MZI as function of phase change, $\Delta\phi$ showing the fringe pattern and the associated intrinsic problems for determination of $\Delta\phi$ from the measured output response known as “sensitivity fading”	65
2.23	Double sensitivity with the use of Bragg grating at the output end of MZI. Light is reflected by bragg grating and thus double the path length of light passing through the sensing window. This method virtually double the interaction length of sensing window	71
2.24	Calculated sensitivity of IO-MZI as function of N_g and waveguide thickness, H with interaction length of 15mm and TE-polarized light with wavelength of 633nm	72
2.25	Calculated sensitivity of IO-MZI as function of wavelength, λ and waveguide thickness, H with interaction length of	73

	15mm, TE-polarized light and waveguide index, N_g of 2.0.	
2.26	Calculated sensitivity of IO-MZI as function of waveguide thickness, H and interaction length, L_{int} with the selected TE-polarized light, wavelength of 633nm and waveguide index, N_g of 2.0	75
2.27	Summary of parameters that affect the performance of IO-MZI biosensor	77
3.1	Amplitude (a) and phase (b) of guided mode viewed in x-z plane by using 3D-FD BPM with semi-vectorial (SV) formulation	81
3.2	Effective index approximation is used to transform 3D optical waveguide into 2D optical waveguide	82
3.3	Process flow for design and simulation of IO-MZI biosensor	85
3.4	Schematic of IO-MZI with the length parameters, L and loss parameter, α of each component.	91
4.1	Single-mode condition (maximum allowable rib width for monomode) of rib waveguide as function of rib depth, d and rib thickness, H with a W resolution and a d resolution of $0.1\mu\text{m}$ and 2nm respectively. The wavelength and polarization used are 632.8nm and TE-polarization respectively. Results for TM polarization are almost similar with TE polarization. The well-known single-mode condition of Soref et al. (Soref et al., 1991) is shown (dashed line -----) for comparison	94
4.2	(a) Penetration depth of evanescent field as function of thickness for both TE and TM polarization. Calculated penetration depth of an equivalent slab waveguide (dashed line ---) is shown for comparison. (b) Penetration depth as function of rib width for thickness of 75nm and 250nm respectively. Different type of data point represents different rib depth	95
4.3	a) Normalized output power of IO-MZI as function of cover index change for thickness of 75 and 250nm respectively. Fitting of the simulation result with the power function (represented by dashed line ---) is performed to obtain actual sensitivity of waveguide. See the inset for the simulated XZ distribution of IO-MZI with thickness of 250nm at phase of π (b) Comparison between simulated and calculated sensitivity of IO-MZI	96
4.4	XZ field intensity of IO-MZI when $\Delta\varphi = \pi$ for rib width of	97

4 μm (a) and 3 μm (b) with rib height of 250nm and rib depth of 2nm.

- 4.5 Correlation between bulk sensitivity and evanescent field penetration depth for TE and TM polarization. Calculated value is shown for comparison 98
- 4.6 Comparison of waveguide mode with thickness of 75nm (a) and 250nm (b) with the dark line indicates the boundary of rib waveguide. The penetration depth of mode into cladding and substrate layer is 1 μm and 1 μm and 0.5 μm for waveguide thickness of 75nm and 250nm respectively 99
- 4.7 Power transfer ratio as function of bending length for WG_75 and WG_250. See the inset for the simulated XZ distribution of Y-branch splitter. Separation of Y-branch splitter is 100 μm . The optimized bending length for WG_250 and WG_75 are 2mm and 5mm respectively 100
- 4.8 (a) Basic structure of vertical taper used to convert the mode size of SMF with the waveguide IO-MZI. (b) Simulated YZ field intensity of vertical taper. 101
- 4.9 (a) Insertion loss of rib waveguide with Gaussian beam of 4.7 μm in mode size as function of input rib waveguide thickness. See the insets for modal distribution of SMF and input rib waveguide of different thickness. (b) Insertion loss of mode-size converter as function of taper length for WG_75 and WG_250. See the inset for YZ distribution and structure of mode-size converter 102

LIST OF NOMENCLATURE

μ TAS	Miniaturized total analysis system
3D	Three dimensions
AC	Alternating current
AFM	Atomic force microscopy
AFRIM	Armed Forces Research Institute of Medical
Ar	Argon
ASSURED	Affordable; Sensitive; Specific; User-friendly; Rapid; Equipment free; Delivered to those who need it
BAW	Bulk acoustic wave
BPM	Beam propagation method
CDC	Center for disease control
CF	Complement fixation test
CF ₄	Tetrafluoromethane
CFR	Case fatality rate
CMOS	Complementary metal-oxide silicon transistor
CMOS	Complementary metal-oxide-semiconductor
dB	Decibels
DC	Direct current
DENV	Dengue virus
DF	Dengue fever
DHF	Dengue hemorrhagic fever
DI	Deionized water
DL	Detection limit
DSS	Dengue shock syndrome
ELISA	Enzyme linked immunosorbent assay

F-20	Filmetric 20
FCCS	Fluorescence cross-correlation spectroscopy
FD-BPM	Finite difference beam propagation method
FET	Field effect transistor
FFT	Fast fourier transform
FWHM	Full width at half maximum
GIS	Geographical information system
GOF	Goodness of fit
HI	Hemagglutination inhibition assay
HPM	High power microscope
HRP	Horse-raish peroxidase
ICP	Inductive coupled power
ICT	Immunochromatography
IgA	Immunoglobulin A
IgE	Immunoglobulin E
IgG	Immunoglobulin G
IgM	Immunoglobulin M
IO	Integrated optic
IO-MZI	Integrated optical Mach-Zehnder Interferometer
IUPAC	International Union of Pure and Applied Chemistry
JEV	Japanese encephalitis virus
LED	Light emitting diode
LPCVD	Low pressure chemical vapor deposition
LSPR	Long range SPR
MZI_250	MZI with waveguide thickness of 250nm
MZI_75	MZI with waveguide thickness of 75nm
NAAT	Nucleic acid amplification test

NEP	Noise equivalent power
NS1	Non-structural protein 1
OFIS	Optical fiber immunosensor
PCR	Polymerase chain reaction
PMT	Photomultiplier tube
POC	Point of care
POI	Power overlap integral
PRNT	Plaque reduction neutralization technique
PVDI	Pediatric Dengue Vaccine Initiative
QCM	Quartz crystal microbalance
RDT	Rapid diagnostic test
RF	Radio frequency
RIU	Refractive index unit
RPD	Relative power versus distance
S/N	Signal to noise ratio
SAW	Surface acoustic wave
SDS	Sodium dodecyl sulfate
SF ₆	Sulfur hexafluoride
Si ₃ N ₄	Silicon nitride
SiON	Silicon oxynitride
SMF	Single-mode fibre
SOI	Silicon-on-insulator
SPR	Surface Plasmon resonance
TBEV	Tick-borne encephalitis virus
TE	Transverse electric
TIR	Total internal reflection
TM	Transverse magnetic

UV	Ultraviolet
VCSEL	Vertical-cavity-surface-emitting laser
WG_250	Rib waveguide with thickness of 250nm, depth of 1nm and width of 4 μ m
WG_75	Rib waveguide with thickness of 75nm, depth of 1nm and width of 3 μ m
WHO	World Health Organization
WNV	West Nile virus
XRD	X-ray diffraction
YFV	Yellow Fever virus
Sensitivity	Sensitivity of IO-MZI sensor which is defined as rate of change of phase of guided mode as cover refractive index varies. $\partial\phi/\partial n_c$
Bulk Sensitivity	Sensitivity of evanescent field on cover layer which is defined as rate of change of effective index of guided mode as cover refractive index varies, $\partial N_{eff}/\partial N_c$
Surface Sensitivity	Sensitivity of evanescent field on adlayer layer which is defined as rate of change of effective index of guided mode as thickness of adlayer varies, $\partial N_{eff}/\partial d_f$

LIST OF SYMBOLS

$\partial N_{eff}/\partial d_f$	Surface sensitivity
$\partial N_{eff}/\partial N_c$	Bulk sensitivity
Δd_f	Change in adlayer thickness
Δn_c	Change in bulk index
ΔN_{eff}	Change in effective index
$\Delta\phi_{min}$	Minimum phase change detectable
A and B	Process coefficient of oxidation process
A and B	Process coefficient of oxidation process
d	Rib depth
d_c	Penetration depth of mode into cladding layer
d_{eff}	Effective thickness
d_s	Penetration depth of mode into substrate layer
E_o	Electric field strength (V/m)
E_m	Electric field intensity
H	Rib height or thickness
h	Height of slab region of rib waveguide
h	Strain of polysilicon
H_x	Lateral width of Gaussian beam
H_c	Cladding thickness
H_m	Magnetic Field
H_o	Thickness of waveguide for single mode behavior
H_{opt}	Optimized thickness
H_s	Substrate thickness

H_y	Vertical width of Gaussian beam
k	wavevector of optical ray
k_x	transverse wavevector
L	Wafer length of simulation window
L_{in}	Input waveguide length
L_y	Y-branch bending length
L_{int}	Interaction length of sensing window
m	Mode index
N_{ad}	Refractive index of antibody
N_c	Refractive index of cladding layer
N_{eff}	Effective index
N_{effm}	Discrete effective index
N_g	Refractive index of guide layer
N_s	Refractive index of substrate layer
N_{si}	Refractive index of silicon wafer
$P(z)$	Power as function of propagation distance
$P_{2\pi}$	Maximum power detectable by photodetector
P_{in}	Power of laser source
P_{min}	Minimum power change detectable
Pol	Polarization
P_{out}	Output power of IO-MZI
P_x	Lateral position of Gaussian beam
P_y	Vertical position of Gaussian beam
S	Sensitivity of IO-MZI
S_{ad}	Surface sensitivity

S_c	Bulk sensitivity of waveguide
S_{sur}	Surface sensitivity
t	Oxidation time
t_{ox}	Oxide thickness
V	Visibility factor of power transfer function
W	Rib width
WTl	Lower wafer thickness of simulation window
WTu	Upper wafer thickness of simulation window
WW	Wafer width of simulation window
α / α_{total}	Total insertion loss
α_{in}	Input insertion loss
α_y	Excess loss of Y-branch splitter
α_p	Propagation loss of rib waveguide
β	Longitudinal wavevector or propagation constant
β_m	Discrete propagation constants
Δx	Lateral mesh for simulation
Δy	Vertical mesh for simulation
Δz	Propagation constant
$\theta_{c,c}$	Critical angle at cladding interface
$\theta_{c,s}$	Critical angle at substrate interface
θ_{im}	Incidence angle of each mode (m th)
λ	Wavelength of laser source
P	Power
ρ	Index for polarization

Interferometer Mach-Zehnder Bersepadu Optik untuk Aplikasi Penderia Biologi

ABSTRAK

Denggi merupakan masalah kesihatan yang semakin ketara dan melibatkan lebih daripada separuh populasi dunia. Disebabkan oleh kepesatan pertumbuhan penduduk dan perubahan iklim dunia, lebih 2.5-3 bilion orang, merangkumi lebih daripada 40% daripada penduduk dunia kini berisiko tinggi untuk menghadapi demam denggi. Malaysia, yang terletak berhampiran dengan garisan khatulistiwa, merupakan salah satu negara yang paling terjejas oleh denggi di rantau Pasifik Barat. Kes-kes demam denggi di Malaysia telah melebihi sasaran negara, iaitu 50 kadar insiden demam denggi bagi setiap 100,000 penduduk sejak 2005 sehingga kini. Kit ujian denggi amat diperlukan kerana ia boleh mempercepatkan process pengesanan awal denggi di mana-mana dengan masa yang singkat. Namun begitu, penggunaan kit ujian ini bagi pengawasan denggi amat terhad kerana disebabkan kos ujian yang tinggi dan kelemahan ketepatan ujian. Oleh sebab itu, kajian ini bertujuan untuk membangunkan penderia biologi yang memenuhi keperluan kit ujian bagi pengawasan denggi terutamanya di negara-negara membangun, di mana sumber adalah terhad. Kajian ini menggunakan teknologi penderia biologi optik tanpa tanda dalam reka-bentuk penderia biologi ini. Reka-bentuk Interferometer Mach-Zehnder bersepadu optik telah dijalankan berdasarkan kaedah simulasi yang menggunakan perbezaan terhingga tiga dimensi secara perambatan alur. Perisian OptiBPM dipilih kerana ia adalah mesra-pengguna dan ia membolehkan simulasi tiga dimensi yang diperlukan dalam kajian ini dilaksanakan. Konsep utama kajian ini adalah untuk mengoptimumkan prestasi Interferometer Mach-Zehnder bersepadu optik melalui pengoptimuman setiap komponen, iaitu pandu gelombang optik rabung, pemecah-Y dan penukar mod-saiz. Prestasi optima telah mencapai had pengesanan 5.448×10^{-7} unit indeks biasan, yang merupakan dapatan yang baru bagi penyelidikan seumpamanya, dengan menggunakan pandu gelombang rabung dengan lebar $3.5 \mu\text{m}$, kedalaman 1nm dan ketebalan 75nm. Tambahan pula, kepekaan penderia ini telah meningkat ke $5011 * 2\pi$ rad disebabkan oleh panjang interaksi yang optima, iaitu 16mm.

Integrated Optical Mach-Zehnder Interferometer for Biosensor Application

ABSTRACT

Dengue is an emerging global health problem affecting over half the world's population. With the rapid pace of population growth and climate change, the population at risk of dengue has reached the figure of 2.5-3.0 billions, approximately 40% of the world's population. Malaysia, a dengue hyperendemic country located near the equator, is one of the most affected countries by dengue in Western-Pacific region. The national target for the incidence rate of DF/DHF cases, 50 cases per 100,000 populations, has long been exceeded since 2005 until now. Rapid diagnostic test is in great demand ever since, however the current RDT is not sufficient as an effective passive surveillance system due to the high cost and lack of accuracy. Hence, this study aimed to develop a dengue RDT that is not only have the characteristics of point-of-care (POC) diagnostic but also suits the criteria needed to achieve a large scale disease surveillance in most developing countries where resources are limited. Label-free optical biosensor had been proposed to realized an ideal surveillance RDT. The design of integrated optic Mach-Zehnder Interferometer (IO-MZI) biosensor had been carried out based on the simulation and fabrication method. Simulation of IO-MZI was carried out by using three-dimensional finite difference beam propagation method with the aim of sensitivity and detection limit optimization. OptiBPM software is selected because it is user-friendly and it allows three-dimensional simulation which is needed in this research. The main concept of this research is to optimize performance of IO-MZI through the optimization of each individual component which are rib waveguide, Y-branch splitter and mode-size converter. The optimized IO-MZI achieved detection limit of 5.448×10^{-7} RIU, which is the novelty of this research, with the use of rib waveguide with width of $3.5 \mu\text{m}$, depth of 1nm and thickness of 75nm . Besides, the sensitivity, S of the IO-MZI biosensor has been improved to $5011 * 2\pi$ rad because of the optimized interaction length of 16mm .

CHAPTER 1

INTRODUCTION

1.1 Background

Dengue is an emerging global health problem affecting over half the world's population (Duane J. Gubler & Clark, 1995; Guzman et al., 2010; Monath, 1994; E.-E. Ooi & Gubler, 2008). Due to the current induced disease burden in developing countries, dengue is considered as neglected tropical disease by World Health Organization (WHO). It is also the most important and widespread arthropod-borne viral infection in tropical and subtropical countries, mostly between latitudes 35°N and 35°S where dengue viruses (DENVs) were easily transmitted by the principal vector, *Aedes aegypti*.

Aedes aegypti, the primary vector of dengue original from Africa had evolved as a peridomestic mosquito species that is highly associated with human habitation (Monath, 1994). Dengue viruses is a flavivirus within the *Flaviviridae* family and there are four distinct serotypes of DENV namely DENV-1, DENV-2, DENV-3 and DENV-4 (WHO, 2009). Each of them can infect human and cause similar spectrum of illness. *Flaviviridae* family contains more than 70 viruses with some of them poses a threat to public health as Yellow Fever virus (YFV), West Nile virus (WNV), Japanese encephalitis virus (JEV) and tick-borne encephalitis virus (TBEV) (Rigau-Perez et al., 1998; Whitehead, Blaney, Durbin, & Murphy, 2007). Non-human primates are the original host of DENVs where the virus evolved slowly and entered urban cycle independently an estimated 500-1,000 years ago (Whitehead et al., 2007). Virus transmission cycle between human and vector mosquito is shown in Figure 1.1. The cycle is started with the non-infective mosquito vector taking a blood meal from a

viraemic person and become infective after an incubation period of 8-10 days (Monath, 1994). The infective mosquito can then easily transmit the DENVs by simply probing the skin or taking a blood meal of humans.

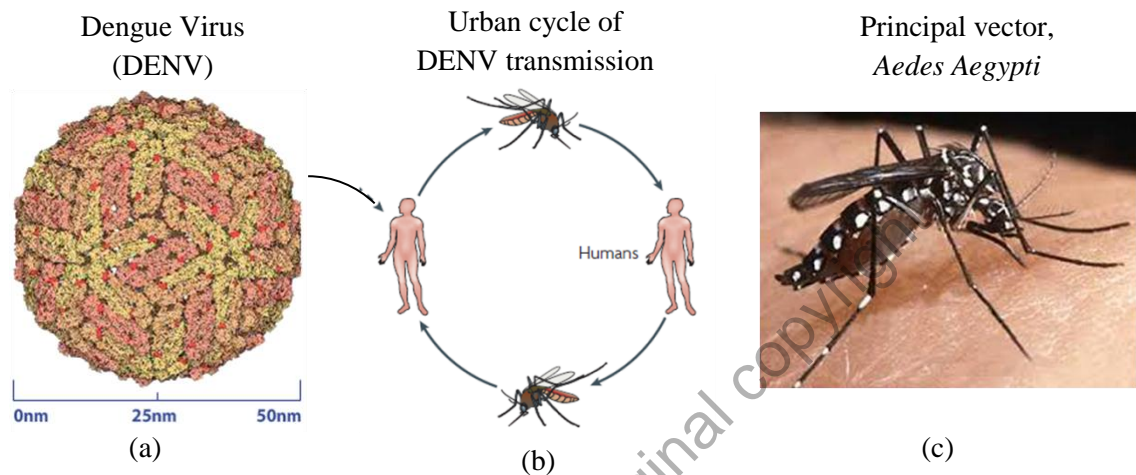


Figure 1.1: Urban cycle (b) of dengue virus (DENV) (a) transmission between *Aedes aegypti* (c) and humans (Whitehead et al., 2007).

After an incubation period of 3-8 days, infection of DENV in human body produce a broad spectrum of clinical presentation ranging from asymptomatic, undifferentiated febrile illness, dengue fever (DF) and more severe dengue hemorrhagic fever (DHF) and dengue shock syndrome (DSS) (Ministry of Health, 2010; WHO, 2009). The non-complicated dengue fever had been recognized for >200 years. The systemic DF is not life threatening but it can be fatal in its severe form; DHF and DSS. These severe dengue had only been recognized recently and the first report of DHF is being made in 1950s. (Whitehead et al., 2007) The case fatality rate (CFR) of DSS is 12-44% and it is this DSS that claims most life of dengue patients (Rigau-Perez et al., 1998).

With the rapid pace of population growth and climate change, the population at risk of dengue has reached the figure of 2.5-3.0 billion, approximately 40% of the world's population (Guzman et al., 2010; PDVI, 2009). According to the report of

Pediatric Dengue Vaccine Initiative (PDVI) (PDVI, 2009), the countries that are contagious with DENVs had reached a figure of 124 countries worldwide with most of them are hyperendemic where 4 dengue serotypes are co-circulating. The distribution of countries or areas at risk of dengue transmission, worldwide in 2008 is shown in Figure 1.2.

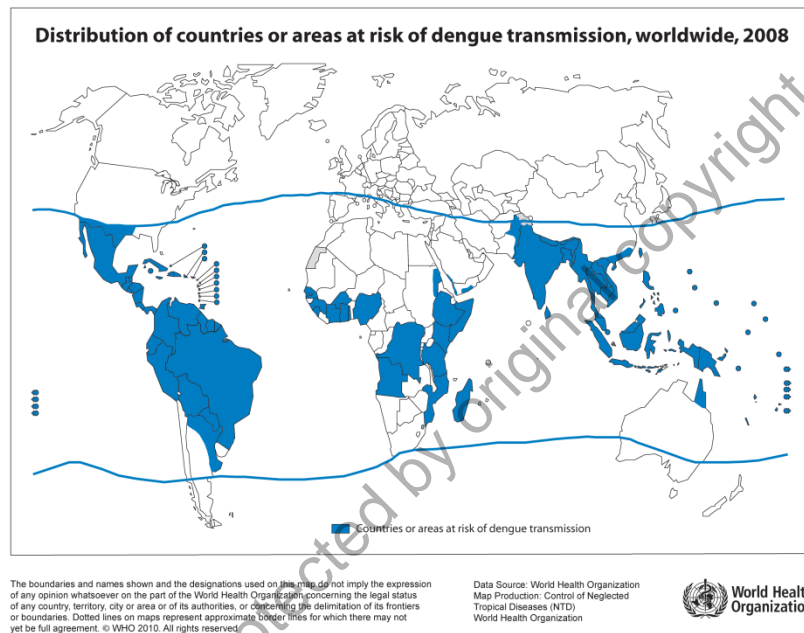


Figure 1.2: Distribution of countries or areas at risk of dengue transmission, worldwide, 2008 with the corresponding co-circulating serotypes (Guzman et al., 2010; WHO, 2008).

The number of dengue cases reported to WHO had been increasing in an exponential trend since 1955 with maximum reported number of 925,896 cases within a period of 2000-2007 as shown in Figure 1.3 (WHO, 2009). Due to the lack of diagnosis test, surveillance and reporting system in most developing countries, the actual number of DF/DHF cases might be several folds higher (Monath, 1994). The report of the United Nations World Tourism Organization in 2004 showed that 125 million international tourists visited countries where there is a risk of dengue infection. The travelling to tropical countries had contributed to another 3-6 million cases according to